

Kepler data on KIC 7341653, a nearby M dwarf with monster flares and a phase-coherent variability

Valeri V. Makarov

valeri.makarov@navy.mil

US Naval Observatory, 3450 Massachusetts Ave NW, Washington DC 20392-5420, USA

Alexey Goldin

alexey.goldin@gmail.com

Teza Technology, 150 N Michigan Ave, Chicago IL 60601, USA

Accepted . Received ; in original form

ABSTRACT

KIC 7341653 is one of several late-type M dwarfs observed in the main mission of Kepler with peculiar infrared colors placing them in the domain of suspected young stellar objects (YSO). It is likely associated with a powerful X-ray emitter with X-ray flares. Kepler light curves reveal two distinct types of activity: frequent flares lasting from less than 30 min to a few hours and a periodic variability with a period of 0.5463441(7) d. The largest flare detected increased the flux in the Kepler passband by a factor of 2.8 and released an estimated 4×10^{34} erg of energy in the Kepler band. Segmented periodogram analysis reveals that the amplitude of the periodic variation was subject to secular changes, dropping from peak values around 20 ppt to below 5 ppt toward the end of the mission, while the phase varied periodically with an amplitude of 0.15 radians and period 362(3) d. Two possible interpretations of the phase periodicity are discussed: a migrating long-lived photospheric spot and a Doppler frequency shift generated by a solar-mass faint companion, such as a white dwarf.

1. Introduction

The star KIC 7341653 drew our attention when we investigated a sample of Kepler main mission targets listed in the selection by Marton et al. (2016) of candidate class I/II/III young stellar objects (YSO), i.e., very young protostellar formations. The authors used near- and mid-infrared photometric data from the 2MASS (Cutri et al. 2003) and WISE (Cutri et al. 2013) catalogs and applied an automated method of machine learning. We found 10 objects of class I/II and 175 objects of class III out of the 133,980 YSO candidates matching Kepler targets with their positions within $10''$. These objects must be interlopers with unusual

infrared photometric properties mimicking those of YSO, since no known regions of ongoing star formation are present in the field of view of Kepler. Even though young stars can be dispersed or ejected out of their parent clusters (e.g., Makarov 2006), the nearest ones are invariably found in loose associations or moving groups (Makarov 2007), because their ages (less than several Myr) are too short for them to travel far. Our original motivation was to see if any extragalactic active galactic nuclei (AGN) could be identified on the Kepler list, due to a partial overlap of YSO and AGN colors in WISE magnitudes (see, e.g., Secret et al. 2015). Instead, we found a versatile collection of stars, some of them quite blue in the optical such as a few A-type main sequence dwarfs, with variable light curves and signs of activity, including small and frequent flares and dips. A smaller group of very red stars stands out with their significant proper motions measured in the URAT1 catalog (Zacharias et al. 2015) and significant ground-based parallaxes (Finch & Zacharias 2016). These stars are nearby late-type M dwarfs typically at 20–50 pc from the Sun.

M dwarfs are very common stars in the Galaxy and in the Solar neighborhood in particular (Henry et al. 2006), but the late-type objects found in the intersection of the lists of YSO candidates and Kepler targets stand out from the general sample in a few respects. Firstly, their unusual MIR colors resulted in the confusion with YSO and imply a significant presence of circumstellar dust. Whether the dust is aggregated in accretion disks similar to the classical T Tauri stars or other types of structures, is not known. Secondly, the selected objects have other signs of activity likening them with pre-main-sequence stars, such as flares and intense X-ray radiation. Many of these objects are cross-matched with the Rosat Bright Source or Faint Source catalogs (Voges et al. 1999, 2000). A brief revision of the Kepler long-cadence light curves reveals frequent flares (probably, of Sun-like, or chromospheric, type), sometimes accompanied with frequent dips of short duration and periodic or quasi-periodic variations. Kepler data on a well-known representative of flaring M5 stars, the binary GJ 1245 A and B, were studied in depth by Lurie et al. (2015), including the total energies and effective duration of flares.

KIC 7341653 has received much less attention in the literature. It is a very red star, with accurately determined AAVSO magnitudes $V = 14.348(55)$ mag and $B - V = 1.549(65)$ ¹ mag (Henden et al. 2016) placing it in the M4 spectral type domain. Riaz et al. (2006) estimate a photometric distance of only 14 pc and a relative X-ray luminosity $\log L_X/L_{\text{bol}}$ of -2.41, indicating a high degree of coronal activity surpassing the saturation limit at ~ -3 . Finch & Zacharias (2016) determined a larger trigonometric distance of 21 pc. Assuming this distance, the flux in the 0.3–10 keV band measured by SWIFT (D’Elia et al. 2013) converts to an X-ray luminosity of 3.14×10^{28} erg s⁻¹, which implies an even higher $\log L_X/L_{\text{bol}}$ of -2.10. The difference between the photometric and astrometric distance moduli of almost 1 mag may indicate the presence of a close, unresolved companion which is fainter than the primary by 0.3

¹Throughout this paper, numbers in round brackets stand for standard errors of values in the last significant digits, i.e., 1.549(65) is equivalent to 1.549 ± 0.065

mag. This hypothetical companion could be a late-type M dwarf, but its presence would still not explain the unusual infrared colors. Riaz et al. (2006) determined a rather low equivalent width of the H_α line, $EW H_\alpha = 1.2 \text{ \AA}$, which is at the low end of the range for magnetically active stars according to West et al. (2004). This modest emission seems at odds with the high level of X-ray luminosity.

The associated X-ray source (1RXS J185504.7 + 425952) was detected by Rosat and included in the catalog of bright sources (Voges et al. 1999). Due to the poor angular resolution of the Rosat telescope ($8''$ in this case), this association can not be a definite proof that the X-ray emission comes from the star in question. Any source within several arcseconds of the star can in fact be responsible for this detection. Fuhrmeister & Schmitt (2003) identified KIC 7341653 as a flaring X-ray source based on the Rosat all-sky survey, which implies a high degree of variability. The Gaia DR1 catalog (Brown & Gaia Collaboration 2016) lists our target at (RA, Dec)J2015 = (283.7690559, +42.9975114) deg, and with $G = 12.633$ mag, but there is a much fainter neighbor in that catalog, source 2105033123254264320, at (283.7700490, +42.9995093), $G = 20.656$ mag, i.e., separated by $7.653''$ in PA=20.0 deg from our target. The Rosat position, for what it's worth, is closer to the bright star's position, but in the catalog of optical/X-ray associations (Flesch 2016), the only source listed (MORX J185504.7+425957) is much closer to the faint Gaia neighbor, and is associated with it. The optical counterpart is considered to most likely be a galaxy. This would seal the fate of this X-ray association perhaps, if not for the more accurate position of the X-ray detection with Swift (Evans et al. 2014) at (283.76943, +42.99797) deg with a 90% radial error of $4.4''$, which is closer to the M dwarf. We should accept that there is no complete certainty in where the large and variable X-ray emission comes from. Fig. 1, center, shows the stacked Pan-STARRS DR1 image centered on the Gaia position of the faint neighbor. A star-like source is clearly seen close to the expected position, but there is another object between it and the target star whose glow is visible in the lower right corner. This faint object, possibly a galaxy, is separated from the M dwarf by approximately $5''.6$ in PA=20° is another candidate for the bright X-ray emission.

The brightest X-ray emitters in the immediate solar neighborhood are predominantly RS CVn-type giants, BY Dra-type main sequence dwarfs, short-period binaries of W UMa type, and pre-main-sequence or T Tauri stars (Makarov 2003). The excess of coronal X-ray emission for these normal field stars is confidently related to a fast rotation caused by either tidal interaction in binaries or a young age. M dwarfs are relatively fainter in X-rays despite the existence of the population of very active, emission-line dMe stars. Even when such magnetically active M dwarfs reach the saturation limit, they can not rival their larger counterparts in the total X-ray coronal emission due to the smaller volume of their coronas. The possible (but not confidently proven) high X-ray luminosity of KIC 7341653 singles it out as a very unusual object. Our original motivation was to find out if Kepler data bore any evidence of close binarity or rapid rotation. To this end, we processed and analyzed the entire sample of Kepler astrometric and photometric data available through the MAST archive hosted at the STScI, covering almost 4 years of continuous observations in the long-cadence regime. The methods of data processing are briefly described in Section 2. Section 3 deals

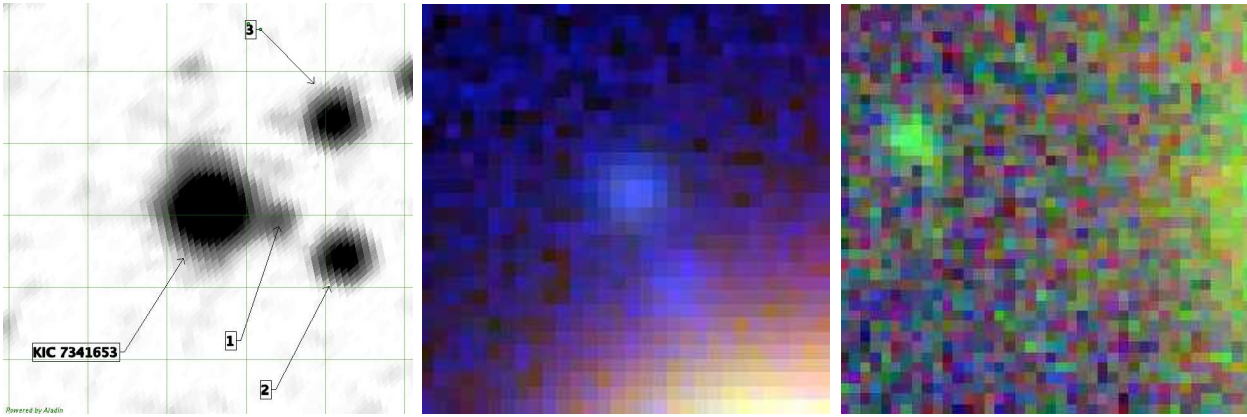


Fig. 1.— Images of the sky at KIC 7341653 and its close surroundings. In all graphs, north is up, east is to the left. Left: Finding chart for KIC 7341653 reproduced using the CDS Aladin v9.0 web tool from the DSS Red survey. The size of a grid square is $10''$. The target star and three neighbors discussed in the paper are labeled. Center: Stacked multi-color Pan-STARRS image of the close vicinity north of KIC 7341653. The glow in the lower right corner indicates the location of the star (outside the imaged area). The size of the image is $7''.5$ on a side. The source close to the center is the 20.7 mag Gaia source 2105033123254264320. The fainter blurred object between the source and the star is not listed in any catalog. Right: Stacked multi-color Pan-STARRS images of the close vicinity east of KIC 7341653, with the same scale as the center chart. The size of the image is $10''$ on a side. The peculiarly shaped faint object has not been seen or listed in any catalogs or surveys.

with photometric flares detected in the PCA-processed light curves. Variability-induced motion (VIM) effects in photometry and astrometry are presented in Section 4. Periodic variations of the light curves are analyzed in Section 5. Interpretation of the results is given in Section 6, and a summary in Section 7.

2. Methods

We use the raw Simple Aperture Photometry (SAP) Kepler light curves rather than the Pre-search Data Conditioning (PDC) fluxes derived by the data processing pipeline (Christiansen et al. 2012). Our aim was to detect possible variations in the data on the time scale up to 90 days. The de-trending procedures based on low-order polynomials to remove the slow variations of flux in the raw data are not always sufficient to mitigate the common instrumental perturbations shared by targets on the same channel. Instead we applied our specially designed Principal Component Analysis (PCA) pre-whitening and filtering procedure described in Makarov & Goldin (2016b). This method allows us to come as close as possible to the intrinsic variability of the star at a level of 20 ppm. We always use 4 principal components for both astrometric and photometric data divided into quarter-year segments (~ 90 days).

We add to our analysis the astrometric data gathered by Kepler, i.e., the photocenter centroids measured at the same cadence and simultaneously with the flux. Synchronous astrometric excursions of centroids, called Variability Induced Motion (VIM), provide a powerful method of detecting double stars or other events of signal blending (Makarov & Goldin 2016a). VIM occurs when one of the blended sources in the aperture is photometrically variable. Since the recorded centroid corresponds to the first moment of the distribution of flux over the pixel grid, which is sensitive to the flux ratio of the blended components, the photocenter moves in a strongly correlated way with the total flux. The published list of VIMs includes 12 confident detections (for 12 mission quarters) with a rather large effective distance of $ds/dF \times F50 \simeq 0''.2$, and VIM directions scattered around 75° on the sky.

3. Monster flares

Fig. 2, left, shows the PCA-filtered 30 min-cadence light curve in Quarter 13 normalized to the median value. The median detected flux is $\sim 93 \times 10^3 \text{ e}^- \text{ s}^{-1}$, which puts the object below the blooming and saturation limits. The standard deviation of the flux values is $\sim 3900 \text{ e}^- \text{ s}^{-1}$. Multiple spikes of variable height indicate flare activity on this star. This does not come as a surprise because mid-M dwarfs are known to have energetic and frequent flares even when their $\text{H}\alpha$ measurements do not indicate an elevated magnetic activity (Hawley et al. 2014). Probably the best studied flaring M dwarfs in the Kepler collection are GJ 1243 (M4) and GJ 1245 AB (M5). The former is especially close to KIC 7341653 by its general characteristics, although it has a higher EW $\text{H}\alpha$. But the flares we find on KIC 7341653 are of immense power compared

to its previously known counterparts, including the famous prototype of the class, UV Ceti (Lovell et al. 1974), and rivaling the BY Dra-type system YY Gem as presented in Lacy et al. (1976). We call them “monster flares” in analogy with the “super-flares” recently suggested for solar-type stars. Table 1 lists the most prominent flares detected in the set of 16 mission quarters with amplitudes confidently exceeding 10% (100 parts-per-thousand, ppt) relative to the quiescent flux. Peak fluxes can only approximately be estimated with the available light curves because of the insufficient time resolution of the 30-min cadence. Likewise, the duration and the total emitted power are roughly estimated. The latter parameter, E_{Kp} in units of erg, is derived following the procedure described in Hawley et al. (2014). Using their specific flux zero-point and the trigonometric parallax, we estimate the quiescent luminosity of KIC 7341653 in the Kepler band at $\log L_{Kp} = 30.70 \text{ erg s}^{-1}$. This is close to the previously estimated $\log L_{Kp}$ for GJ 1243 (30.67). Column 1 specifies the time of peak flux for each flare in mission days, column 2 the peak amplitudes in ppt, column 3 the total energy, $\log E_{Kp}$, in erg, column 4 approximate total duration in hours, and column 5 notes about the structure and associated astrometric signals.

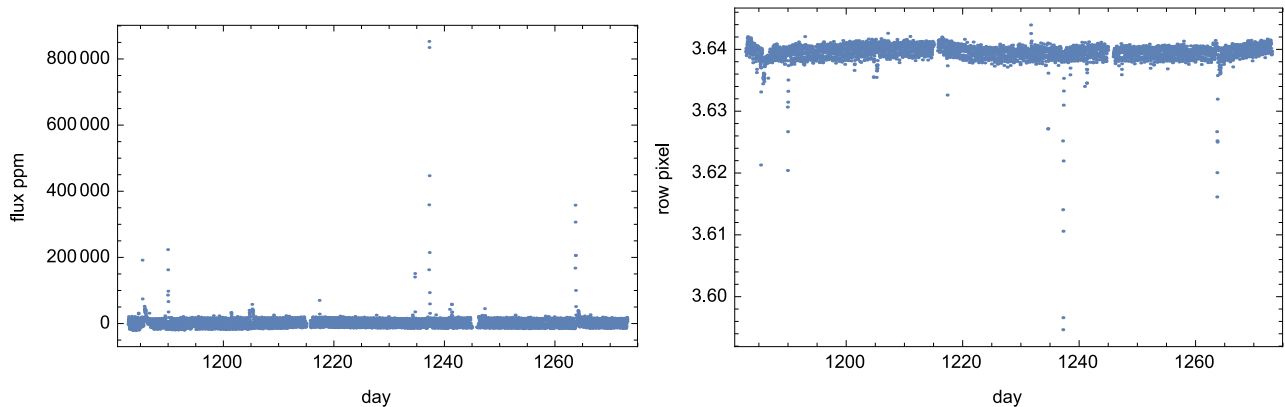


Fig. 2.— PCA-cleaned normalized SAP flux (left) and centroid position in row pixels (right) of KIC 7341653 during mission quarter 13. Multiple flares were observed, mirrored in the centroid position due to a VIM effect.

It is quite remarkable how much energy is released in the flare events on KIC 7341653. These are roughly 30 times more powerful than the flares on the close analog GJ 1243. The largest detected flare on day 1443.1 was so powerful that the flux peaked at 2.8 times the quiescent level. A burst of similar magnitude, if it happened on the Sun, could be catastrophic for the ecosphere on Earth. However, even the greatest “super-flares” observed on solar-type stars (Maehara et al. 2015) fall far behind the energy we observe for KIC 7341653.

The morphology of these powerful flares is diverse. Fig 3, left, depicts a single, short duration flare on day 863.5, characterized by a rapid rise, often not resolved on the 30-min cadence, and a slower exponential decay lasting for one to a few hours. It appears that this sharp and powerful burst in flux is faithfully reproduced in the column pixel coordinate shown

Table 1: Largest flares of KIC 7341653.

Day	Amplitude ppt	$\log E_{Kp}$ erg	Duration hr	Notes
191.1	194	33.7	3.0	
216.4	183	34.2	12.0	complex
275.0	124	33.2	1.5	flare and wave have diff. VIM direction
369.4	187	33.3	2.0	
377.6	155	33.5	1.5	
389.1	158	33.5	4.5	
409.6	140	33.5	2.5	
523.1	204	33.5	2.0	
551.9	177	33.6	2.0	
560.2	134	33.4	3.0	
602.1	133	33.5	2.5	
659.3	570	34.0	2.0	
668.4	508	33.9	2.0	
675.4	314	34.4	10.0	complex
695.6	349	34.1	4.0	
863.5	204	33.3	2.5	
997.5	630	34.6	10.0	double, sep. by 3 hr
1117.5	133	33.4	2.0	
1237.2	834	34.4	5.0	
1263.7	358	34.1	5.0	may be double
1319.5	234	34.2	7.0	complex
1339.8	137	33.3	2.0	
1385.8	106	33.0	1.5	
1391.9	139	33.3	2.0	
1426.4	185	33.5	2.0	
1438.5	142	33.7	5.0	double, sep. 2.5 hr, diff. VIM direction
1443.1	1773	34.6	3.5	most powerful flare detected
1452.3	214	33.5	2.5	
1464.6	338	33.9	6.0	diff. VIM direction
1577.1	104	33.3	2.0	
1579.0	253	33.8	2.5	

in the right panel of the figure. Quite a few flares are distinctly double, with time-resolved peaks, or more complex multiple flares with sometimes gradual rising slopes, such as the one on day 675.4. Only a small fraction ($\sim 10\%$) of flare events have such complex structures, possibly indicating a different physical origin.

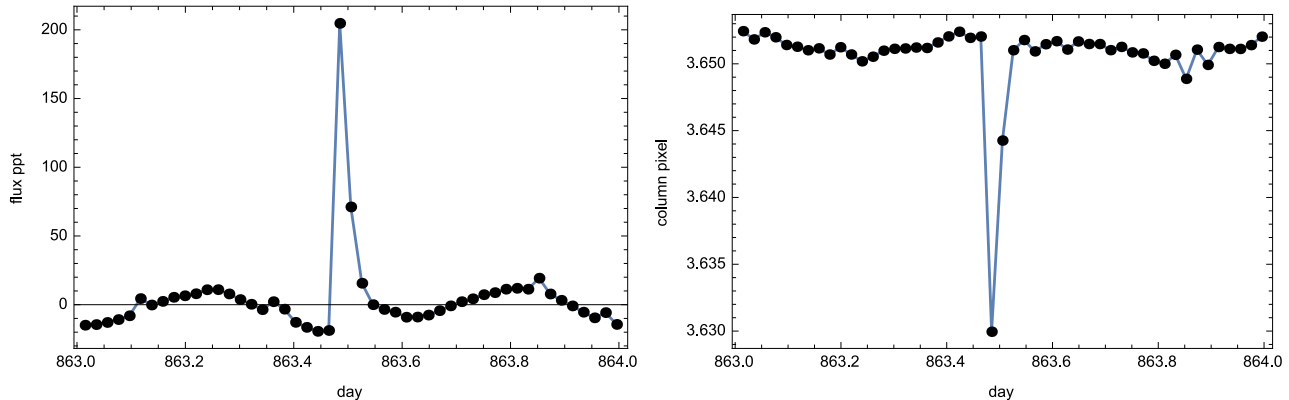


Fig. 3.— PCA-cleaned normalized SAP flux (left) and centroid position in column pixels (right) of KIC 7341653 during the flare event on day 863.5.

4. VIM detections

The *en masse* analysis by Makarov & Goldin (2016a) has already established that KIC 7341653 shows powerful and consistent VIM effects during the entire mission. The prevailing direction of the astrometric perturbations (position angle counted from north through east) is $\sim 75^\circ$. We find a previously unknown, very faint and possibly elongated object approximately in this direction with J2000 coordinates (283.7755, +42.998), separated by $10''.3$ at position angle 82° (Fig. 1, right). This object has not been listed in any catalog or survey. It can be discerned only in heavily stacked Pan-STARRS images, implying a faint magnitude. This enigmatic object can hardly cause the observed centroid motion due to its faintness. The close blue companions in Fig. 1, left, have a position angle inconsistent with the detected VIM direction. Recalling that the VIM vector is inverted when the photometric variability takes place on the target star (i.e., a flare on the target star will move the photocenter toward the target star and away from the blended companion), we should consider the opposite direction to the average VIM vector ($\sim 255^\circ$). We find another, much brighter, neighbor with a Gaia DR1 position (283.76517, +42.99702), separation $10''.38$ at position angle 260.2° , and $G = 19.29$ mag (component 1 in Fig. 1, left). The Pan-STARRS DR1 (PS1) PSF magnitudes for this star are $g = 20.763(20)$, $r = 19.584(11)$, $i = 18.845(6)$, $z = 18.481(11)$, $y = 18.024(11)$ mag, indicating a background early M-dwarf. It is tempting to assign the observed VIM to this companion. A simple calculation of the expected photocenter shift seems to be inconsistent with this interpretation, however. As the companion is approximately 500 times fainter than the target

star, the moment-based centroid should be displaced by roughly $0''.02$ in the quiescent state. No matter how much extra flux comes from a flare on the primary, the astrometric excursion can not exceed this distance. The observed excursions during the largest flares exceed $0''.15$.

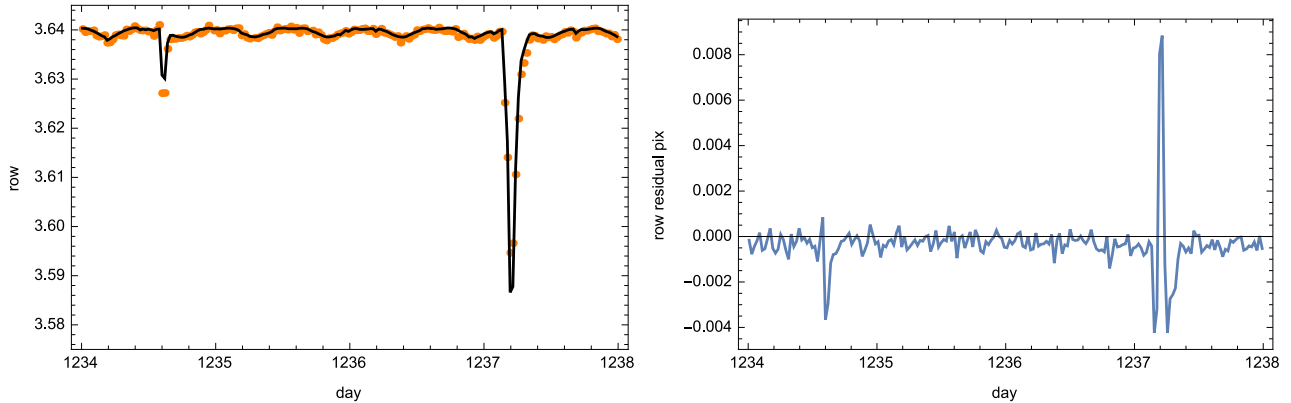


Fig. 4.— Left: PCA-cleaned row pixel coordinates for a segment of long-cadence data including two flares (orange dots) and a least-squares linear fit of the simultaneous light curve (black line, see text). Right: residuals of row centroid measurements after the best fitting linear model based on flux is subtracted.

A much brighter, but also much more distant, neighbor labeled 2 in Fig. 1, left, has also roughly the matching position angle (250.0°). It is separated from the target star by $20''.7$ and has a G magnitude of 17.05. Being ~ 0.017 in flux of the target, this companion could generate a photocenter shift of $0''.35$, if it were completely blended. The digital aperture is large enough (Fig. 5) to accommodate part of the flux from neighbor 2, which can cause a VIM of the observed magnitude because of the asymmetric distribution of light in the truncated image. The elongated shape of the aperture, which varied for the mission quarters, could also explain why this companion, but not the companion 3 of similar brightness at separation $21''.6$, position angle 303.2° (neighbor 3 in Fig. 1) generates the strongest VIM.

Having identified a plausible source of blended flux, we would like to make sure that the powerful flares detected in the light curve do not come from this chance companion. Firstly, we note that the brightest flare on day 1443 raised the flux by a factor of 2.8, which would imply an increase by 5.5 magnitudes if it comes from the companion. Although flares of such magnitude have been recorded for most active binaries of BY Dra and RS CVn type, companion 2 does not seem to be a plausible source with its Sun-like colors ($g_{\text{PS1}} - r_{\text{PS1}} = 0.44$ mag). Secondly, flare images do not show any obvious asymmetry one should expect from a source separated by ~ 5 pixels from the target. Fig. 5, left, shows the differential distribution of pixel flux during the peak of day 1237.2 flare event in absolute units of electrons per second, i.e., the difference in flux between the maximum of that flare and the median flux over the entire Q13 data, for each pixel. The center of the stellar image is in pixel (5, 4). The distribution of additional flux seems to be consistent with the quiescent flux distribution and centered on the target star.

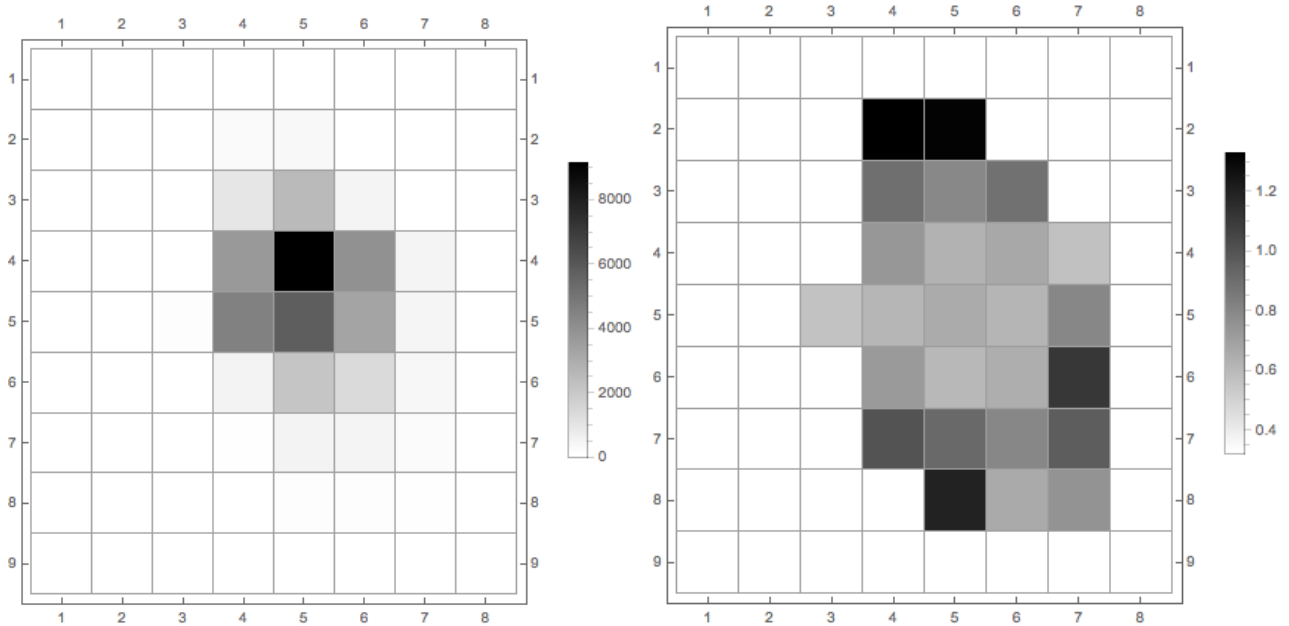


Fig. 5.— Left: Intensity-coded pixel flux registered during the flare on day 1237.2 in excess of the median pixel values over that quarter. The units are $e^{-} s^{-1}$. Right: the same flare flux but relative to the median flux distribution. The shaded area shows the star- and quarter-specific digital aperture used both for astrometry and photometry.

The same data expressed in relative units, i.e., $(f_{\text{flare}} - f_{\text{quiescent}})/f_{\text{quiescent}}$, tells a different story (Fig. 5, right). While the total flux increased by 83% during this flare (Table 1), some pixels on the fringes became brighter by a larger fraction, and this enhancement is observed on both sides of the image. This implies that the shape of the image changed during the flare, not just the amplitude. The two relatively brightest pixels, (4, 2) and (5, 2), defined the VIM direction for this event, but the enhancement of flux in the counter direction is fairly obvious too. Such bizarre structures may occur, for example, if the subtracted sky background or dark current value are overestimated, artificially reducing the level of starlight in pixels. The VIM direction is expected to be resilient to this error, but it may alter the VIM magnitude by putting additional flux outside the blended companion. Another possibility is a nonlinear response of pixels to increasing incident flux due to saturation. Saturation effects in Kepler data have been encountered and discussed by Lurie et al. (2015); Luger et al. (2016). Our target star is significantly fainter than the $Kp = 11.3$ mag which is believed to be the saturation threshold (Gilliland et al. 2010). However, scientific CCDs are known to have an interval of nonlinear quantum response before the full well saturation is achieved (Janesick 2001). It is possible that the most energetic flares drive the brightest pixels into the pre-saturation nonlinear regime. The full well of the Kepler CCD is approximately 10 000 DN (van Cleve et al. 2009), and at a typical inverse gain of $110 e^{-}/\text{DN}$, the corresponding pixel flux is $\sim 180\,000 e^{-} s^{-1}$. We can find some support to this hypothesis in Fig. 4 which shows the observed light curve (black line) fitted to the observed centroid position in row coordinates (orange points) for a segment

with two flares. While the fitted flux undershoots the centroid motion for the small flare on day 1234.6, it overshoots the shift during the peak of the large flare on day 1237.2. This can also be seen in the residuals of the fit in the right plot of Fig. 4. This systematic behavior is found for the entire set of flares. It is a worrying result, because it implies an onset of nonlinear response somewhere between 23 000 and 30 000 $e^- s^{-1}$, which is a much lower value than previously assumed.

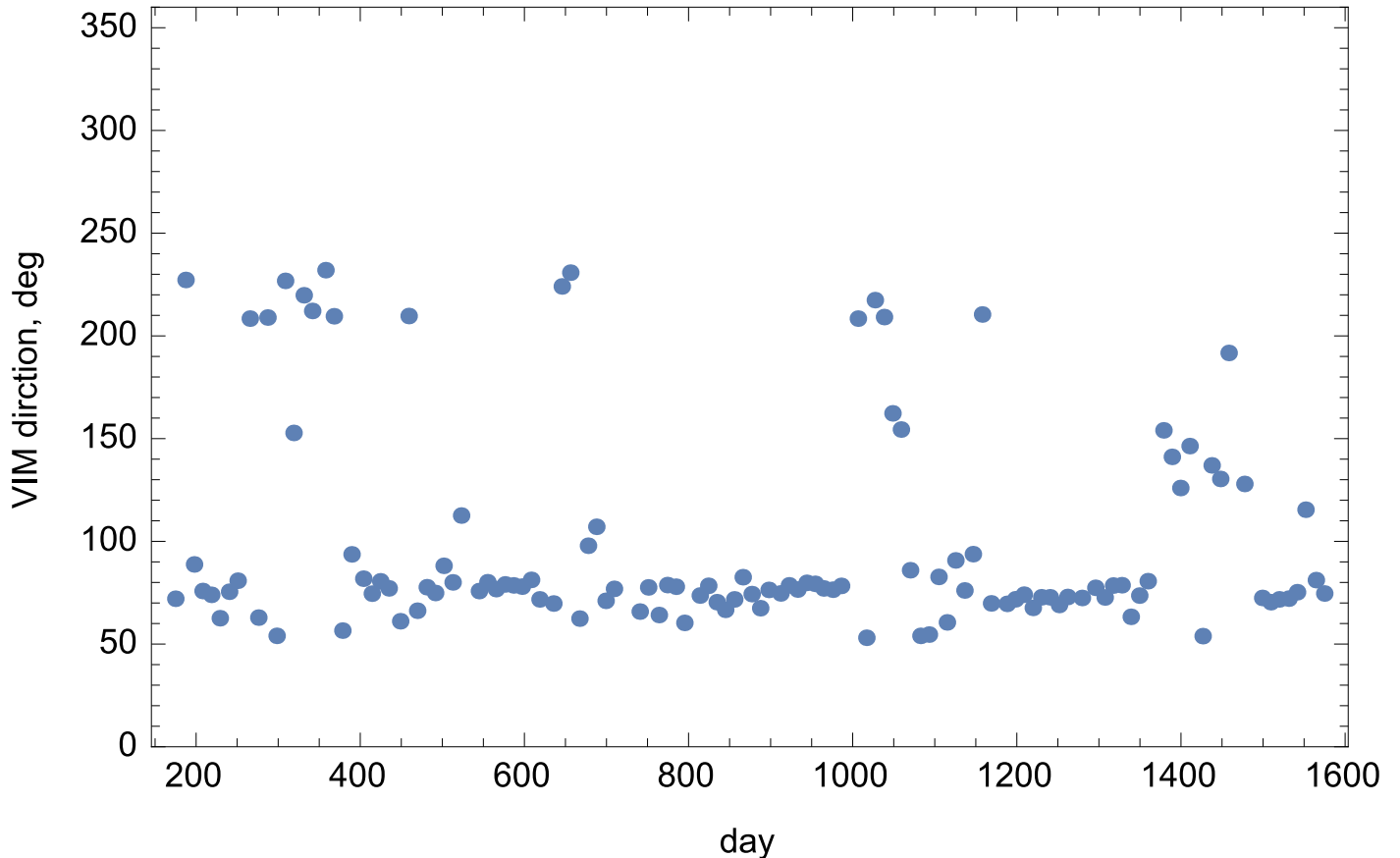


Fig. 6.— VIM directions in sky position angles calculated for bins of 500 consecutive measurements (flux and centroid coordinates) over the entire collection of 16 mission quarters.

We suggest an alternative explanation to the aureole of fractional flux generated by a bright flare. Pixels of a CCD do not have physical boundaries but are delineated by so-called depletion zones where the quantum efficiency drops to zero. As charge is accumulated in a pixel, the depletion zones shrink (Plazas et al. 2017). The boundary between two adjacent pixels will shift toward the pixel with more accumulated charge, effectively reducing its collecting area. A fraction of photons will therefore be re-distributed between the pixels, with the fainter one collecting relatively more light. This phenomenon is dubbed the “brighter-fatter” (BF) effect (Antilogus et al. 2014). It is not visible in regular flat-field images of uniform intensity, but can be quite large for small-scale astronomical images such as point-like sources

(Smith & Rahmer 2008). E.g., the fractional difference between a long and a short exposures of the same source (light spot) shows a lower peak and broader wings of the bright spot, which generate a doughnut-shaped distribution of light (Guyonnet et al. 2015). If this interpretation holds, the BF aureole for Kepler star images is very wide, extending to $\sim 5\text{--}6$ pixels in diameter. Due to the elongated shape of the digital aperture, some fraction of the redistributed extra charge may fall outside the collecting area. The photometric effect will be limited to the spillage of charge at the wings of the image, causing a small decrease of the total signal. Astrometric effects are more significant, changing the magnitude of observed motion to higher values. As a conclusion, the so-called VIM speed parameter may be exaggerated by the BF effect and carry little information about the configuration of blended sources.

With this caveat in mind, we consider in greater detail the direction of the VIM motion. Fig. 6 shows VIM position angle determinations for the whole long-cadence data set covering 4 years. Each point corresponds to a bin of 500 non-overlapping observations. The estimation was done differently from the previous analysis by Makarov & Goldin (2016a). The coordinate measurements in x (column) and y (row) for each bin were fitted with a straight line using the orthogonal regression method (Makarov & Goldin 2016b). The slope of this line defines the coordinate direction which is converted into a sky position angle using the WCS parameters in the metadata. Most of the short-term estimates cluster around a $\text{PA} = 75^\circ$, in a good agreement with the previous quarterly estimation by a different method. But there are occasional intervals where the VIM direction switches to a much different value, which is $\sim 220^\circ$ in the first half of the mission gradually converging with the stable direction toward its end. This bifurcation can be explained by the presence of a third blended component with an azimuthal motion around the target star. We thus find a clue to the existence of an orbiting companion with a period of longer than 4 years. The magnitude of VIM depends on the amplitude of photometric variability, and if the hypothetical companion is variable, it can sometimes dominate the observed motion despite the smaller separation.

5. Periodic variation of flux

We performed multiple periodogram computations parsing the PCA-cleaned light curve into segments of various length, as well as the entire mission. The most energetic flares were clipped for a better characterization of the periodic wave (visible in Fig. 4, for example). A powerful peak was invariably obtained at a period ~ 0.5464 d, with smaller secondary and tertiary harmonics clearly present, indicating a non-sinusoidal oscillation. Unlike KOI-54, the prototype of the Heartbeat stars (Welsh et al. 2011), where the main peak splits in two for a sufficiently long interval of data, our dominating signal remains unresolved in frequency in all the periodograms. Fig. 7 depicts a regular unweighted Lomb’s periodogram of the oscillating light curve for three quarters of the mission combined. The peak with an amplitude of 12 ppt remains single and unresolved suggesting a single-frequency periodic modulation. This separates the star in question from the heartbeat class with tidally excited pulsation and high-

eccentricity binary companions. On the other hand, the phase seems to be remarkably stable and coherent during the entire 4 years of observation. A long-term coherent phase is usually associated with binarity and orbital motion. In analogy with the eclipse time variation (ETV) method which reveals dynamical perturbation from tertiary companions of eclipsing binaries (Borkovits et al. 2016), the phase of a periodic flux signal can be estimated for consecutive segments of the light curve.

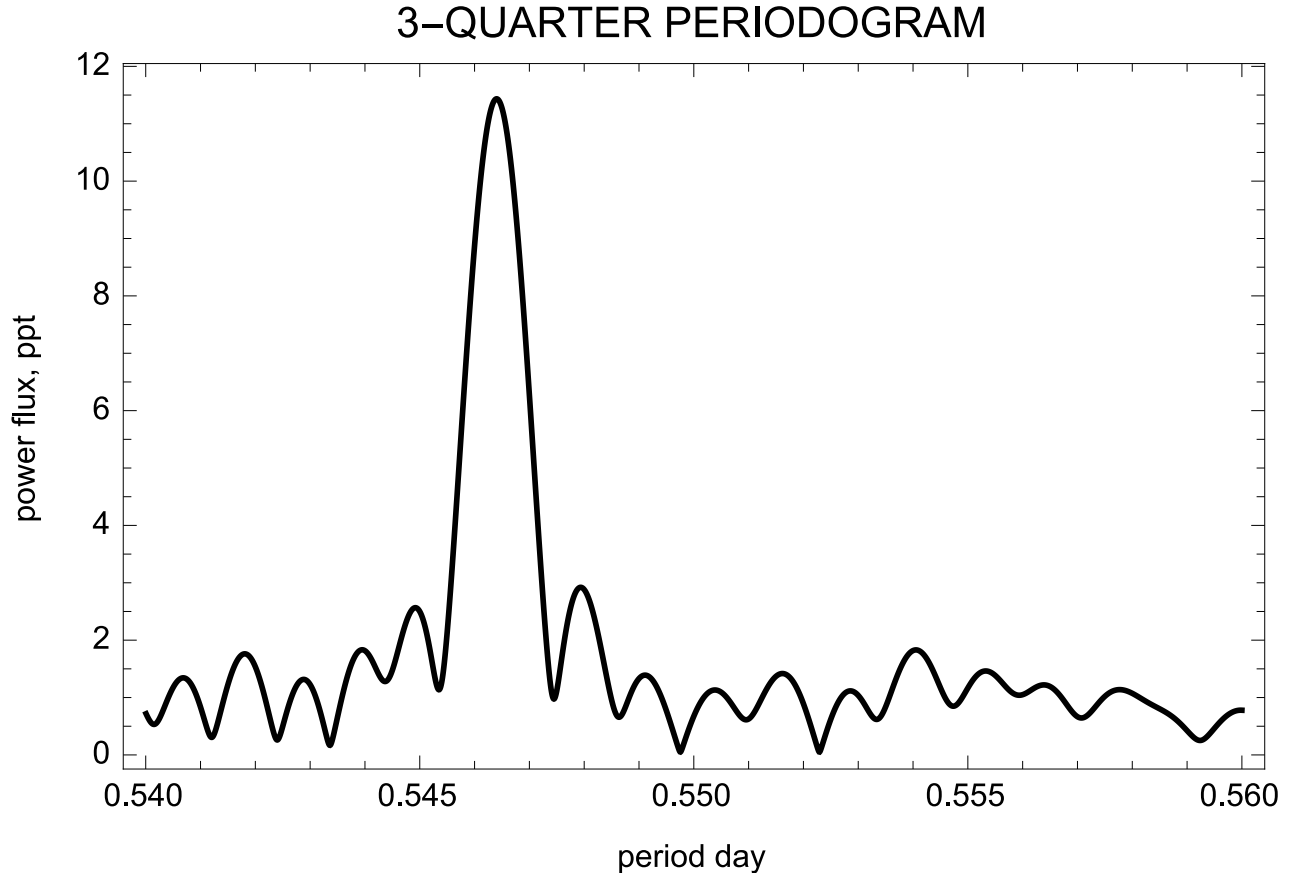


Fig. 7.— High-resolution Lomb’s periodogram of the joined light curve for 3 consecutive mission quarters, Q13 – Q15. The dominating peak at period 0.5464 d remains unresolved, and its width is roughly consistent with the windowing function.

We divide each quarter into intervals of 9 days long (typically, 10 intervals per quarter) and compute a Lomb’s periodogram fit with a fixed period of $P = 0.54634$ d, clipping the flux to ± 30 ppt around the median value to remove the largest flares. The phase of this dominating oscillation was then computed for each interval as $\arctan(a_c, a_s)$, where a_c and a_s are the coefficients of the fit for the model functions $\cos(2\pi t'/P)$ and $\sin(2\pi t'/P)$, respectively. The times t' are shifted to a common zero-point approximately in the middle of the mission, i.e., $t' = t - 1000$, which helps to de-correlate the phase and frequency for the entire collection of observations. Fig. 8 shows segmented phase estimates in degrees across the entire mission. We find surprisingly large variations which look systematic and periodic. It resembles the

strictly periodic signals in ETV data for eclipsing stars which are caused by the Doppler effect or the light travel time effect (sometimes inaccurately called Rømer effect) due to the orbital motion of the target around a third body, i.e., in triple systems (see, e.g., Conroy et al. 2014). In our case, whatever the source of the Doppler delay is, a stable single-frequency flux signal (irrespective of its origin) can be phase-modulated by a barycentric radial velocity variation. However, a full-scale periodogram analysis of the same segments of data with period as a free parameter does not show any periodic variation, being quite flat in time with a mean of 0.54642, median 0.54638, and standard deviation 0.00065 d. This discrepancy is puzzling because a physical Doppler effect should change both the frequency and phase, since the former is the time derivative of the latter. Certainly, the sensitivity of the phase determinations is much greater because the amplitude of modulation gets multiplied by its frequency in the corresponding period modulation, which is a small number. From the half-amplitude and frequency of modulation in Fig. 8, the main mode period is expected to be modulated by roughly 0.4%, or 0.00021 d. This is indeed difficult to detect given the random error of period determinations. Hence, a Doppler-like modulation may be present in the segmented period estimates but we do not see it.

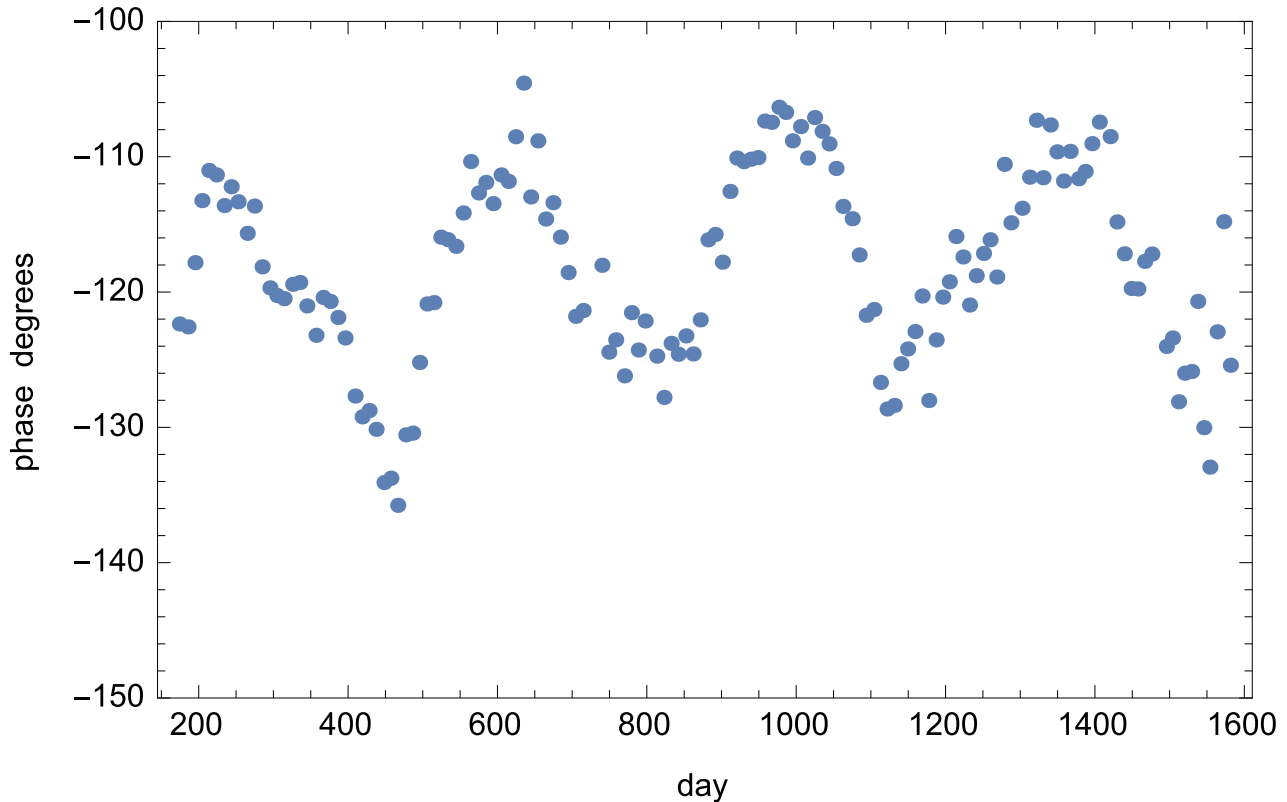


Fig. 8.— Phases of the main oscillation with period 0.54634 d computed for 9 days-long segments of the PCA-cleaned light curve. The zero-point of phase determinations is day 1000.

The amplitude of oscillations significantly varies with time too – see Fig. 9. The amplitude

is computed as the RSS of the estimated coefficients for the main mode, $a = \sqrt{a_c^2 + a_s^2}$. There is no obvious periodicity, but the amplitude strongly declines toward the end of the mission. In addition to the oscillating pattern the light curve also features numerous flares with amplitudes greatly exceeding the oscillation amplitude. This makes the least-squares model of flux vulnerable to perturbations and potentially dependent on many additional parameters. To avoid fitting too many parameters we are not interested in, we tried to use a model where the amplitude is not present at all.

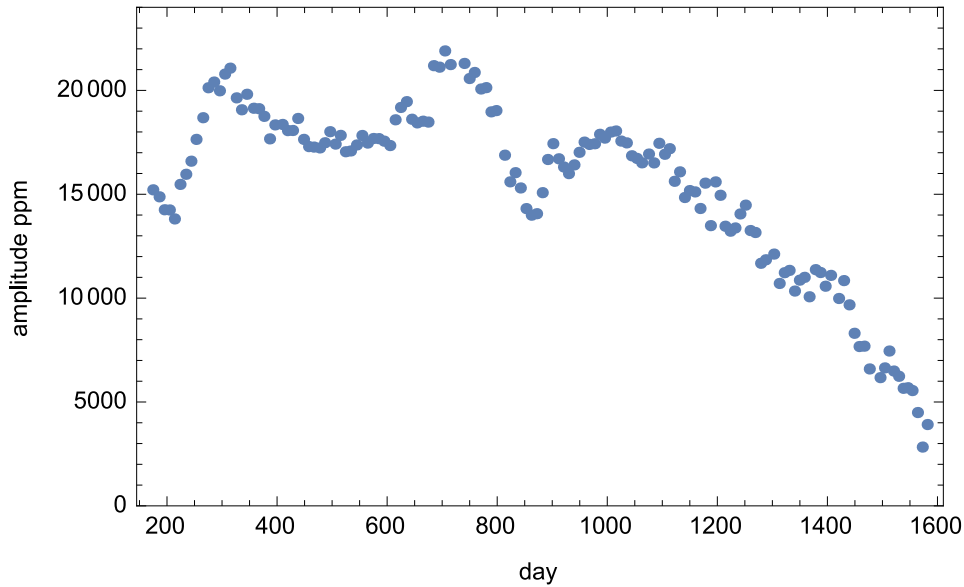


Fig. 9.— Amplitude of the dominating mode of flux oscillation with periods around 0.5464 d.

For each quarter, we determine the median flux f_m and set an auxiliary variable z :

$$z = 0 \text{ if } f < f_m$$

$$z = 1 \text{ if } f \geq f_m$$

We then fit a logistical model:

$$p(z = 1) = \frac{1}{1 + e^{-x}}$$

$$p(z = 0) = \frac{e^{-x}}{1 + e^{-x}}$$

where

$$x = s \cos(\Omega_{osc}t + \phi) \tag{1}$$

$$\phi = \phi_0 + A_\phi \cos(\Omega_\phi t + \phi_\phi) \tag{2}$$

with s being a scale parameter, Ω the frequency, and ϕ the phase of the high-frequency oscillation. A_ϕ is the amplitude of phase variation, Ω_ϕ is the phase variation frequency. This model is simplified in the sense that it includes only a single harmonic of the phase variation rather than a Fourier series, and the main harmonic of the flux oscillation, but it will prove adequate in the following analysis.

This likelihood parametrization has certain advantages. There is no need to fit a time-dependent phase amplitude. We also avoid fitting the possibly variable shape of flux oscillations and a special treatment of numerous flares and upward spikes in the light curve. The log-likelihood function

$$\log L(s, \Omega, \phi_0, A_\phi, \Omega_\phi, \phi_\phi) = \sum_i \log p(z_i) \quad (3)$$

is sampled by the Markov Chain Monte-Carlo package EmCee (Foreman-Mackey et al. 2013). The resulting density plots of the log-likelihood function of the free parameters in Eq. 1 using 160000 samples after discarding initial 100000 burn-in samples are shown in Figs. 10, 11. The fit is well-defined with this model with tight and round-shaped confidence areas. The fitting parameters and their 95% confidence intervals are summarized in Table 2.

T_{osc}	0.5463441	$+7.3 \cdot 10^{-7}$ $-7.2 \cdot 10^{-7}$
ϕ_0	1.8257	$+0.0061$ -0.006
s	5.466	$+0.008$ -0.009
T_ϕ	361.68	$+3.02$ -2.97
A_ϕ	0.150	$+0.008$ -0.009
ϕ_ϕ	1.664	$+0.06$ -0.06

Table 2: Fitted parameters

6. Interpretation

Periodic variations of flux are not infrequent at the sensitivity level of the Kepler photometric data. They can be caused by a number of physical phenomena, but generally, the basic underlying mechanisms are related to 1) intrinsic pulsations; 2) rotation and nonuniform surface brightness distribution; 3) binarity effects. Even though pulsations of different excitation origin were theoretically predicted, they proved to be too small for a positive detection with Kepler even in dedicated short-cadence observations (Rodríguez-López et al. 2014). Besides, the predicted periods of pulsations are considerably shorter than our main oscillation mode (0.5463441(7) d). In the following discussion, we will omit this possibility due to the null result of previous studies.

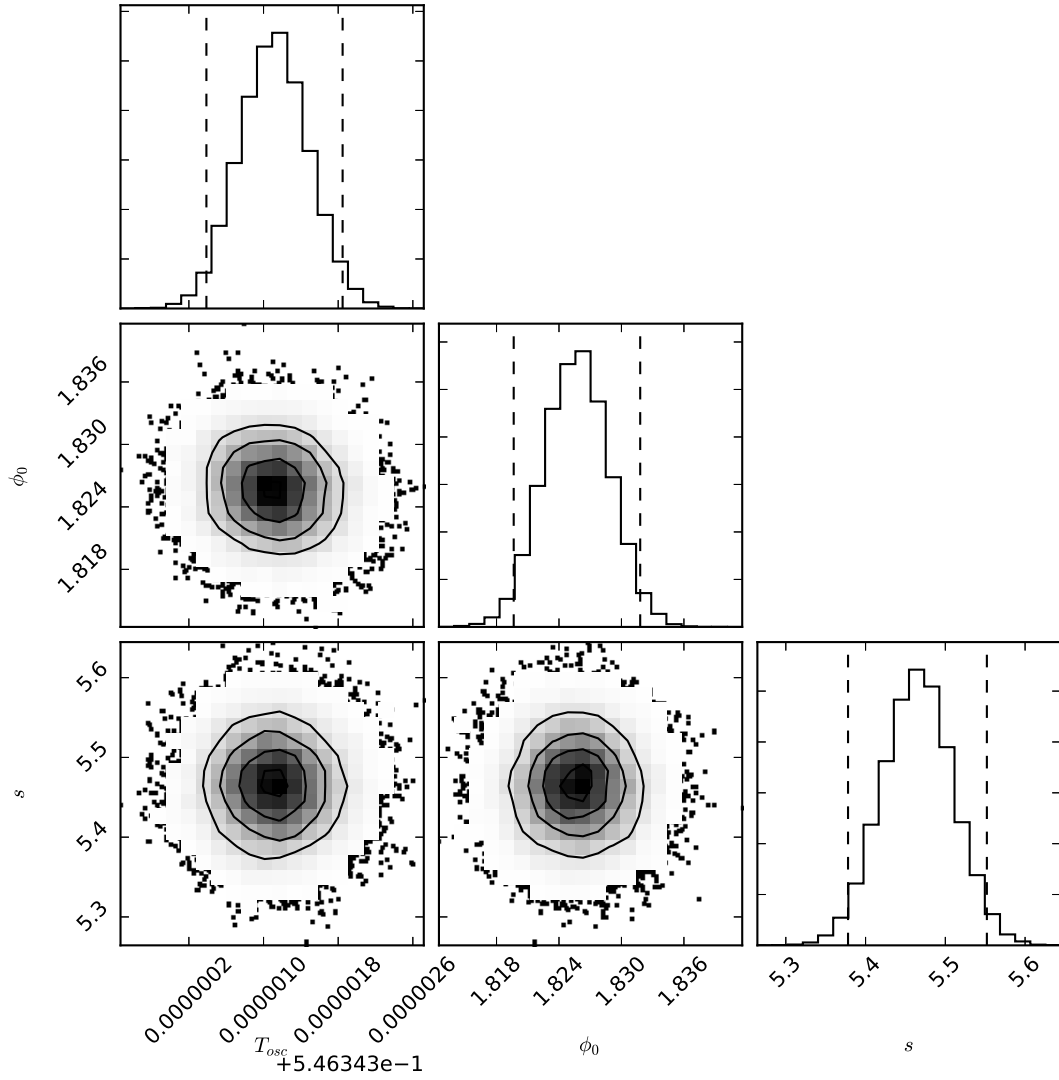


Fig. 10.— Projections of log-likelihood distribution for flux oscillation period T_{osc} , flux oscillation phase and scale s .

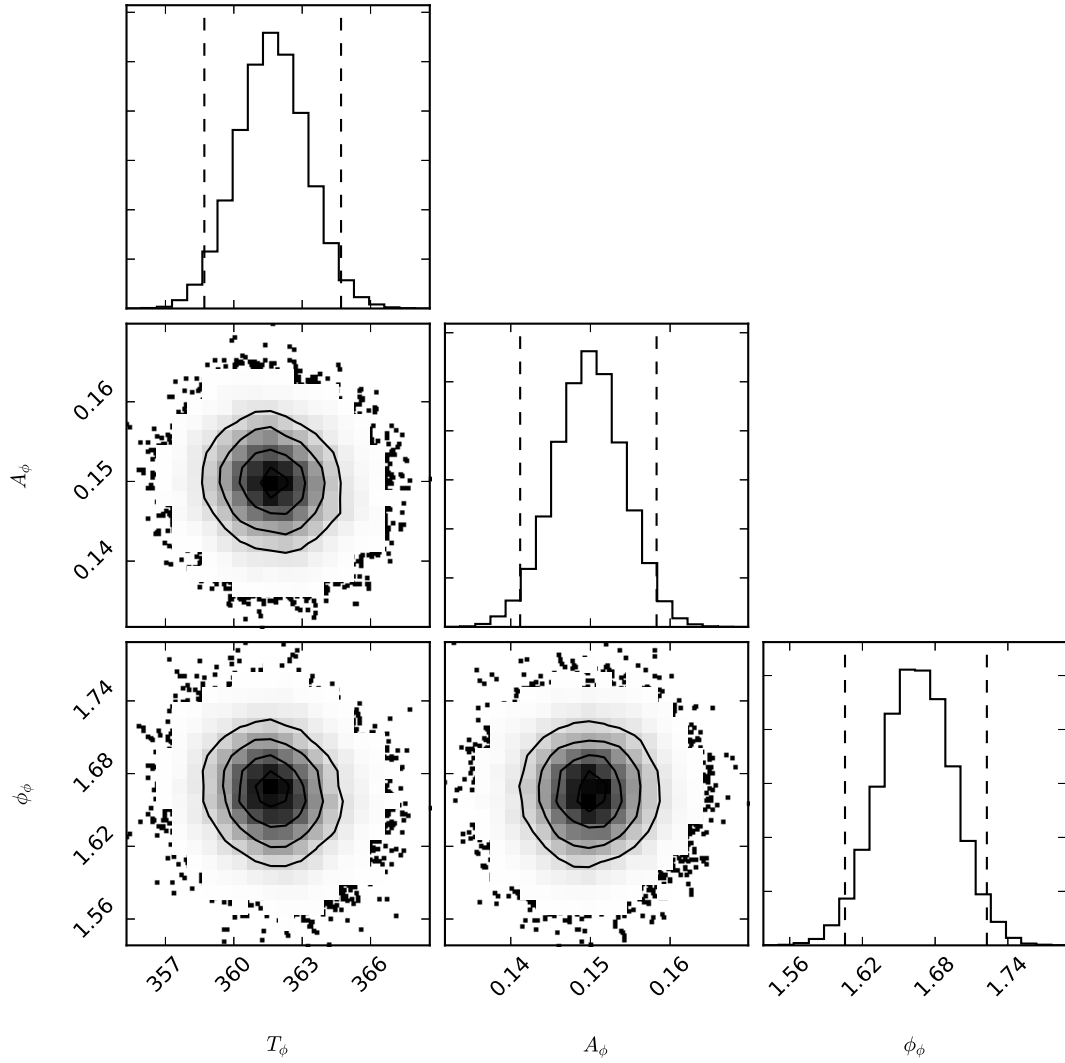


Fig. 11.— Projections of log-likelihood distribution for phase period T_0 , phase amplitude A_ϕ , and phase ϕ_0 .

The remaining two causes, binarity and rotation/activity, may often be interrelated. The rate of rotation and magnetic activity of main sequence dwarfs slows down with age due to rotation braking (Skumanich 1972; Barnes 2003), but this process can be arrested and reversed in tight binary stars by the angular momentum transfer via tidal energy dissipation (e.g., Eggleton et al. 1998). As a result, binaries with orbital periods below a certain threshold (a few days, depending on the spectral type and evolutionary status) are practically all synchronously rotating (Levato 1976). The characteristic time of spin-down for single M dwarfs is ~ 400 Myr (Stauffer et al. 1987). If a single M dwarf is older than the age of the Hyades, it is expected to rotate with a longer period than the observed value for KIC 7341653.

Binary M-dwarfs, on the other hand, can acquire and maintain fast rotation rates for billions of years. The tidal evolution of the orbit is directed toward gradual circularization and further tightening of the orbit. The tidal friction, however, drops to zero for a completely circularized and synchronized binary of zero obliquity (Hut 1980). Such tidal equilibrium pairs remain fast-rotating and, therefore, magnetically active for their lifetimes, because the reservoir of orbital kinetic energy is still large. How can an originally wider pair reach this state without the assistance of significant tidal dissipation? Kiseleva et al. (1998) proposed a mechanism where a tertiary companion, if significantly inclined with respect to the inner orbit generates secular oscillations of the inner orbit’s eccentricity and inclination and boosts the tidal dissipation in the inner pair. This mechanism finds support in the observation that most active binaries known to us often reside in hierarchical multiple systems (Makarov & Eggleton 2009). The emerging interpretation of KIC 7341653 consistent with this scenario is a hierarchical triple system with a mid-type M dwarf as the optically brightest component whose fast rotation is driven by a non-eclipsing secondary, and a sufficiently massive, more distant tertiary component.

It would be tempting to explain the quasi-periodic variations of phase we see in Fig. 8 as the direct consequence of the orbital motion of the inner binary about the tertiary via the light travel time effect (LTTE). Using formulae from Murphy et al. (2014), adjusted to direct phase measurements, we performed a linear optimization fitting for the following Keplerian LTTE model:

$$\phi(t) = \frac{4\pi a_0 \sin i}{cT_{osc}} \left[\cos \omega \frac{\sqrt{1-e^2}}{e} \sum_{k=1}^{\infty} \frac{J_k(ke) \sin knt}{k} + \sin \omega \sum_{k=1}^{\infty} \frac{J_{k-1}(ke) - J_{k+1}(ke)}{2k} \cos knt \right] \quad (4)$$

where a_0 is the semimajor axis of the observed oscillating star, c is the speed of light, i is the inclination of the orbit to the line of sight, ω is the argument of pericenter, e is the eccentricity, n is the mean motion ($n = 2\pi/P_{orb}$), and J_k is the Bessel function of the first kind. The fitting parameters in this model are $a_0 \sin i$, ω , and e . From the former, we can estimate the lower bound mass of the outer companion if we assume a certain mass of the inner binary (or single oscillator) from Kepler’s third law. Our best fit provides an $a_0 \sin i = 117(6) \times 10^6$ km and an eccentricity consistent with 0 but uncertain to 0.1. Assuming a mass of $0.2 M_{\odot}$ for the target star, the mass of the hypothetical 362-day orbiter is $0.77 M_{\odot}$. Since this companion is fainter

in the optical, it could be a white dwarf or a neutron star.

There is significant evidence putting this interpretation of the phase variations in doubt. The curve in Fig. 8 appears more complex than the simple sinusoid our Keplerian fit has produced. There may be other signals of non-cyclic nature present. The 0.546-day oscillation is not perfectly sinusoidal either, which is seen in the light curve (Fig. 3) and is confirmed by periodograms where we find conspicuous second and third harmonics with periods $T_{osc}/2$ and $T_{osc}/3$. Irrespective of the nature of this non-sinusoidal oscillation, an LTTE effect should modulate the frequency of these harmonics too, resulting in a similar cyclic variation of their phase. We performed a similar segmented phase determination for the second harmonic of oscillation and the result (not shown in this paper for brevity) indicates large-amplitude smooth variation that is quite dissimilar to the sinusoid with a 362-day period. This means that not only the phase and amplitude of the main oscillation wave vary, but also its shape.

These peculiar properties are easier explained in the framework of a large brightness feature on the rotating surface, such as a giant spot. Can stellar spots live for longer than 4 years? While most sunspots exist only for days to weeks, active RS CVn-type binaries were found to have long-lived, giant spots with an average lifetime of 2.2 yr, stretching to 4.5 yr (Strassmeier et al. 1994; Strassmeier 2009). Generally, tight binaries sport longer-lived spots than quiescent single stars. A star can have a polar cap-like large spot living for decades if its meridional flow is faster than the solar flow (Holzwarth et al. 2006). Tran et al. (2013) suggested a persistent near-pole hot spot on the surface on a differentially rotating inclined star to explain the anti-correlated eclipse timing variations observed with Kepler for contact binaries. Differential rotation with the equatorial region rotating systematically faster than the polar regions, is believed to be the direct consequence of the Coriolis force acting on convective turbulence (Kitchatinov 2005), so it can be common for M stars. The secular decrease of the amplitude of the main oscillation mode in Fig. 9 can be explained as regular decay of the giant spot toward the end of the main mission (although the exact physical processes involved there are not well understood even for sunspots). The different behavior of the second oscillation harmonic whose pronounced amplitude and phase variations are not correlated with the main mode, can be reasonably expected if the shape and brightness distribution changed in the course of 4 years of observation.

The main challenge to this hypothesis is the cyclic behavior of the phase of main mode oscillation (Fig. 8). Generally, the phase variation may be caused by a persistent active region or a spot migrating or drifting on the surface in longitude, or, in combination with a differential rotation, in latitude. Both directed drifts will effectively change the observed frequency of flux variations. The open issue is what kind of process can make this migration be quasi-periodic in time. The period of variation 362(3) d is perhaps too short to be related to a possible intrinsic magnetic activity cycle. The character of main mode phase variation suggests a periodic component of the surface rotation rate, i.e., libration. If the high rate of rotation is maintained by a close low-mass companion, and there is a more massive tertiary companion on a much wider, inclined orbit, the libration of the pericenter argument of the inner orbit prescribed by

the Lidov-Kozai mechanism (Eggleton et al. 1998; Kiseleva et al. 1998; Kirk et al. 2016) can cause such periodic rotational acceleration. Even in the framework of the spot hypothesis, a hierarchical triple system remains most suitable to explain the peculiar properties of KIC 7341653.

7. Summary

We consider it unlikely that KIC 7341653 is very young such as a T Tauri star or a YSO. The closest young stars to the Sun are identified in loose moving groups and usually have wide companions with approximately the same space velocity and age. No such moving group members have been suggested in the Kepler field. Aside of the unusual infrared colors, the star is likely to be a powerful and variable source of X-ray radiation with giant X-ray flares. We also detect super-flares in the optical Kepler band, with the largest event on day 1443 releasing $\sim 4 \times 10^{34}$ erg of energy within 3.5 hours. These properties put the mid-type M dwarf in the category of extremely active UV Cet-type stars. The energy released during the largest flare is similar to the event detected by Osten et al. (2016) for DG CVn in the optical bandpass.

Our astrometric VIM analysis reveals that each flux variation is rather closely mirrored in the detected centroid position (Fig. 3). This indicates the presence of blended sources in the digital apertures of the target star. The dominating VIM effect probably comes from a rather distant, partially blended source (companion 2 in Fig. 1), but a more detailed view suggests at least one additional source which seems to have a significant azimuthal motion with respect to the target (Fig. 6). Thus, the first clue of binarity or multiplicity of KIC 7341653 comes from Kepler astrometry. Unfortunately, the amplitudes and shapes of the most significant VIM effects are altered by what we suspect to be a manifestation of the “brighter-fatter” effect, which also puts in question the directional information.

The short-period quasi-sinusoidal flux periodicity can be traced across the entire mission span, but its amplitude and phase underwent large secular changes. As the phase shows large-amplitude quasi-periodical variations, the amplitude appears to be fairly constant during the first half of the mission span, then declining from peak values of 20 ppt to less than 5 ppt (Fig. 9). Could the time-variable component in VIM direction and the oscillation amplitude behavior come from the same physical process? In principle, the quasi-period phase modulation with a period of 362(3) d can be explained as a Doppler shift (LTTE) due to the orbital acceleration around a sufficiently massive (at least, $0.77 M_{\odot}$) companion, but the amplitude decay does not seem to be consistent with this interpretation. A more plausible scenario involves a giant spot or an activity region on the photosphere of the fast-rotating star. This would also account for the dissimilar changes in the phase and amplitude of the second harmonic of the 0.54634 d oscillation. The finding at odds with this interpretation is the cycling character of the phase variations. A more sophisticated model may be required to explain the scope of properties, such as a hierarchical triple system with a tight inner binary (but not eclipsing) and a more distant tertiary causing the pericenter argument to librate around 90° or 270° via the Lidov-

Kozai mechanism (Eggleton et al. 1998). We propose such a system as our best educated guess, because it also explains the fast rotation of the M dwarf and its high degree of activity. The tidal dissipation of kinetic energy due to a periodic boost to the inner pair’s eccentricity causes the orbit shrink, increasing the rate of rotation of the tidally synchronized components. The model is consistent with the highest levels X-ray and flaring activity observed in close BY Dra and RS CVn systems.

What could be the nature of the hypothetical companion to KIC 7341653? A matching ultraviolet source is found in the deep GALEX survey of the Kepler field by Olmedo et al. (2015). The measured near-UV magnitude (N_{UV}) is 20.412(44) mag. Assuming a distance of 21 pc, the absolute near-UV magnitude is $M_{NUV} = 18.8$ mag. With the accurate Gaia DR1 magnitude $G = 12.633$, the visual color $N_{UV} - G = 7.78$ mag which places the star far to the left (too blue) of the well-defined main sequence constructed for nearby dwarfs (Makarov, 2017, in preparation). The expected color at this absolute magnitude is 10.04 mag. The difference is too large to be associated with the elevated level of magnetic activity observed in a small fraction of nearby M dwarfs and is more likely to indicate the presence of a hot degenerate companion. The absolute N_{UV} magnitude for such photometrically blended M–WD pairs is close to that of the WD component. This allows us to tentatively estimate the spectral type at D6, i.e., a relatively cool and evolved WD. Morgan et al. (2016) find that at late spectral types (M4–M6), WD+dM pairs flare 50% as frequently as field dMs.

The ultimate judgement on whether a solar-mass companion exists in the system will be delivered by accurate radial velocity measurements. KIC 7341653 was part of a spectroscopic survey conducted by Terrien et al. (2015a,b), but unfortunately, only one determination was obtained for this object (R. Terrien 2016, priv. comm.). A follow-up K2 photometric series would also be useful to determine if the short-period oscillation of flux has died out, or, otherwise, if its phase is still consistent with the value observed during the main Kepler mission.

Acknowledgments

This paper includes data collected by the Kepler mission. Funding for the Kepler mission is provided by the NASA Science Mission directorate. Some of the data presented in this paper were obtained from the Mikulski Archive for Space Telescopes (MAST). STScI is operated by the Association of Universities for Research in Astronomy, Inc., under NASA contract NAS5-26555. Support for MAST for non-HST data is provided by the NASA Office of Space Science via grant NNX09AF08G and by other grants and contracts. This research has made use of “Aladin sky atlas” developed at CDS, Strasbourg Observatory, France. This work has made use of data from the European Space Agency (ESA) mission *Gaia* (<http://www.cosmos.esa.int/gaia>), processed by the *Gaia* Data Processing and Analysis Consortium (DPAC, <http://www.cosmos.esa.int/web/gaia/dpac/consortium>). Funding for the DPAC has been provided by national institutions, in particular the institutions par-

icipating in the *Gaia* Multilateral Agreement. This research has made use of the VizieR catalogue access tool, CDS, Strasbourg, France. The original description of the VizieR service was published in A&AS 143, 23

REFERENCES

- Antilogus, P., Astier, P., Doherty, P., Guyonnet, A., Regnault, N. 2014, *J. of Instrumentation*, 9
- Barnes, S. 2003, *ApJ*, 586, 464
- Borkovits, T., Hajdu, T., Sztakovics, J., et al. 2016, *MNRAS*, 455, 413
- Brown, A. G. A., Vallenari, A., Prusti, T., and Gaia Collaboration, 2016, *A&A*, 595, 2
- Christiansen, J.L., Jenkins, J.M., Caldwell, D.A., et al. 2012, *PASP*, 124, 1279
- Conroy, K.E., Prša, A., Stassun, K.J., et al. 2014, *AJ*, 147, 45
- Cutri, R.M., Skrutskie, M.F., Van Dyk, S., et al. 2003, *The 2MASS All-Sky Catalog of Point Sources*, IPAC/California Institute of Technology
- Cutri, R.M., et al. 2013, *VizieR Online Data Catalog*, 2328
- D’Elia, V., Perri, M., Puccetti, S., et al. 2013, *A&A*, 551, 142
- Eggleton, P.P., Kiseleva, L., Hut, P. 1998, *ApJ*, 499, 853
- ESA 1997, *The Hipparcos and Tycho Catalogues*, ESA SP-1200
- Evans, P.A., Osborne, J.P., Beardmore, A.P., et al. 2014, *ApJS*, 210, 8
- Finch, C., Zacharias, N. 2016, *AJ*, 151, 160
- Flesch, E.W. 2016, *PASA*, 33, 52
- Foreman-Mackey, D., Hogg, D.W., Lang, D., Goodman, J. 2013, *PASP*, 125, 306
- Fuhrmeister, B., & Schmitt, J.H.M.M. 2006, *A&A*, 403, 247
- Gilliland, R.L., Jenkins, J.M., Borucki, W.J., et al. 2010, *ApJ*, 713, L160
- Guyonnet, A., Astier P., Antilogus, P., Regnault, N., Doherty, P., 2015, *A&A*, 575
- Hawley, S.L., Davenport, J.R.A., Kowalski, A.F., et al. 2014, *ApJ*, 797, 121
- Henden, A.A., Templeton, M., Terrell, D., et al. 2016, *VizieR Online Data Catalog: AAVSO Photometric All Sky Survey (APASS) DR9*

- Henry, T.J., Jao, W.C., Subasavage, J.P., et al. 2006, AJ, 132, 2360
- Holzwarth, V., Mackay, D.H., Jardine, M., 2006, MNRAS, 369, 1703
- Hut, P. 1980, A&A, 92, 167
- Janesick, J.R. 2001, *Scientific Charge-Coupled Devices*, SPIE - The International Society for Optical Engineering, Bellingham, Washington
- Kirk, B., Conroy, K., Prša, A., et al. 2016, AJ, 151, 68
- Kiseleva, L.G., Eggleton, P.P., Mikkola, S. 1998, MNRAS, 300, 292
- Kitchatinov, L.L. 2005, Phys. Uspekhi, 48, 449
- Lacy, C.H., Moffet, T.J., Evans, D.S. 1976, ApJS, 30, 85
- Luger, R., Agol, E., Kruse, E., et al. 2016, AJ, 152, 100
- Lurie, J.C., Davenport, J.R.A., Hawley, S.L., et al. 2015, ApJ, 800, 95
- Lomb, N.R. 1976, Ap. Space Sci., 39.447
- Levato, H. 1976, ApJ, 203, 680
- Lovell, B., Mavridis, L.N., Contadakis, M.E. 1974, Nature, 250, 124
- Maehara, H., Shibayama, T., Notsu, S., et al. 2015, Nature, 485, 478
- Makarov, V.V. 2003, AJ, 126, 1996
- Makarov, V.V. 2006, AJ, 131, 2967
- Makarov, V.V. 2007, ApJS, 169, 105
- Makarov, V.V., Goldin, A. 2016, ApJS, 224, 19
- Makarov, V.V., Goldin, A. 2016, ApJ, 833, 78
- Makarov, V.V., Eggleton, P.P. 2009, ApJ, 703, 1760
- Marton, G., Tóth, L.V., Paladini, R. 2016, MNRAS, 458, 3479
- Morgan, D.P., West, A.A., Becker, A.C. 2016, AJ, 151, 114
- Murphy, S.T., Bedding, T.R., Shibahashi, H., et al. 2014, MNRAS, 441, 2575
- Olmedo, M., Lloyd, J., Mamajek, E.E., et al. 2015, ApJ, 813, 100
- Osten, R.A., Kowalski, A., Drake, S.A., et al. 2016, ApJ, 832, 174

- Plazas, A.A., Shapiro, C., Smith, R., Rhodes, J., Huff, E. 2017, arXiv: 1703.08205
- Riaz, B., Gizis, J.E., Harvin, J. 2006, AJ, 132, 866
- Rodríguez-López, C., Gizis, J.E., MacDonald, J. 2014, MNRAS, 446, 2613
- Skumanich, A. 1972, ApJ, 171, 565
- Secrest, N.J., Dudik, R. P., Dorland, B. N., et al. 2015, ApJS, 221, 12
- Smith, M., & Rahmer, G. 2008, SPIE Conf. Series, 7021
- Stauffer, J.R., Hartmann, L.W., Latham, D.W. 1987, ApJ, 320, L51
- Strassmeier, K.G., Hall, D.S., Henry, G.W. 1994, A&A, 282, 535
- Strassmeier, K.G. 2009, Astron. Astroph. Rev., 17, 251
- Terrien, R.C., Mahadevan, S., Bender, C.F., Deshpande, R. Robertson, P. 2015, ApJ, 802, L10
- Terrien, R.C., Mahadevan, S., Deshpande, R. Bender, C.F. 2015, ApJS, 220, 16
- Tran, K., Levine, A., Rappaport, S., et al. 2013, ApJ, 774, 81
- van Cleve, J., Caldwell, D., Thompson, R., et al. 2009, *Kepler Instrument Handbook*, KSCI-19033-001
- Voges, W., Aschenbach, B., Boller, T., et al. 1999, A&A, 349, 389
- Voges, W., Aschenbach, B., Boller, T., et al. 2000, IAU Circ., 7432, 1
- Welsh, W.F, Orosz, J.A., Aerts, C., et al. 2011, ApJS, 197, 4
- West, A.A, Hawley, S.L., Walkowicz, L.M., et al. 2004, AJ, 128, 426
- Zacharias, N., Finch, C., Subasavage, J., et al. 2015, AJ, 150, 101

